IEEE Access
Multidisciplinary | Rapid Review | Open Access Journal

Received July 17, 2019, accepted August 3, 2019, date of publication August 20, 2019, date of current version September 3, 2019.

Digital Object Identifier 10.1109/ACCESS.2019.2936444

Let You See in Sand Dust Weather: A Method Based on Halo-Reduced Dark Channel Prior Dehazing for Sand-Dust Image Enhancement

ZHENGHAO SHI[1], (Member, IEEE), YANING FENG[1], MINGHUA ZHAO[1], ERHU ZHANG[2], AND LIFENG HE[3], (Senior Member, IEEE)

[1]School of Computer Science and Engineering, Xi'an University of Technology, Xi'an 710048, China
[2]School of Digital Media and Engineering, Xi'an University of Technology, Xi'an 710048, China
[3]School of Information Science and Technology, Aichi Prefectural University, Nagakute 4801198, Japan

Corresponding authors: Zhenghao Shi (ylshi@ xaut.edu.cn) and Lifeng He (helifeng@ist.aichi-pu.ac.jp)

This work was supported in part by the National Natural Science Foundation of China under Grant 61872290.

ABSTRACT The images that are captured in sand storms often suffer from low contrast and serious color cast that are caused by sand dust, and these issues will have significant negative effects on the performance of an outdoor computer vision system. To address these problems, a method based on halo-reduced dark channel prior (DCP) dehazing for sand dust image enhancement is proposed in this paper. It includes three components in sequence: color correction in the LAB color space based on gray world theory, dust removal using a halo-reduced DCP dehazing method, and contrast stretching in the LAB color space using a Gamma function improved contrast limited adaptive histogram equalization (CLAHE), in which a guided filter is used to improve the artifacts of the histogram equalization. Experiments on a large number of real sand dust images demonstrate that the proposed method can well remove the overall yellowing tone and dust haze effect and obtain normal visual colors and a detailed clear image.

INDEX TERMS Normalized Gamma correction (NGC), DCP, CLAHE, color correction, LAB color space, illumination enhancement.

I. INTRODUCTION

Images that are captured during sand storms usually suffer from low contrast, noise, and color distortions due to the scattering and absorption of light rays by dust particles. Compared with red and orange light, blue and green light are absorbed by sand dust particles much more quickly. This leads to a color deviation image with an overall yellow tone. Moreover, the light that is absorbed by dust reduces the energy of light rays, which leads to underexposed images, as illustrated in Figure 1(a). This seriously affects the performance of outdoor computer vision systems. Therefore, a method that enhances sand dust images for computer vision applications is highly desired. To address this problem, many studies have been proposed [1]–[13], including using histogram equalization and its variants to stretch images' contrast [1]–[6], using Retinex-based methods to enhance images' contrast and brightness [7], or tackling the sand dust enhancement problem as a dehazing problem [11]–[14].

The associate editor coordinating the review of this article and approving it for publication was Gerardo Di Martino.

Though there are varying degrees of success for the image contrast enhancement methods, almost of all of the methods that are mentioned above still suffer from the following limitations.

Traditional image enhancement methods that are independent of a physical model, such as histogram equalization and Retinex-based methods, usually fail to restore scenes with large depth of field changes where the contrast is more seriously degraded.

(2) Existing dehazing-based methods that are dependent on the image degradation model for hazy images are insufficient for addressing color deviations due to an overall yellow tone in sand dust images. The hazy imaging model usually assumes that the ambient illumination is globally consistent. Therefore, most dehazing methods estimate a white ambient light from the brightest region in the image. However, sand dust scenes usually have overall yellow tones, which causes obvious various and nonuniform colored ambient illumination. This not only makes the estimation of the ambient light inaccurate but also causes some image priors to become invalid. For example, the dark channel prior assumes that

FIGURE 1. Illustration of an image captured in a sand storm and its corresponding enhanced image. left: Sand dust image, and right: Results using our method.

the pixels with the lowest intensity correspond to the black objects in the scene. This prior works well for hazy images, but it cannot be directly applied to sand dust scenes since the lowest intensity may be affected by the overall yellow tone.

To address above mentioned problems, a halo-reduced DCP dehazing-based method for sand dust degraded image enhancement is proposed in this paper. The motivation of our method comes from the following observations (1) Sand dust images share similar optical characters with hazy images, such as atmospheric scattering and absorption. (2) The most different image character between a sand dust image and a hazed image is color. If we scan a similar hazy color dust image, then we can directly employ the existing dehazing method for dust haze removal. (3) Usually, a DCP dehazed image has low illumination, which results in part of the image details being too dim to observe. Based on what was analyzed above, we constructed our method with the following three components in sequence: gray world-based color correction in the LAB color space, dust removal using a halo reduced DCP dehazing method, and contrast stretching in the LAB color space using a Gamma function improved CLAHE. Experiments on real sand dust images show that the proposed method can obtain good color fidelity, good contrast and proper brightness. Figure 1 (b) illustrates an example of our sand dust image enhancement result.

To sum up, our contributions in this paper are the following.

(1) We propose a LAB color space gray world-based image color correction method. By adjusting the a and b chromatic components, a natural color image can be obtained.

(2) We propose halo-reduced dark channel prior dehazing for dust haze removal. To expand the image contrast, a Gamma function improved CLAHE in the LAB color space is developed in which a guided filter is applied to improve the artifacts of histogram equalization.

The structure of the remainder of this paper is as follows. In Section II, the related works are adequately explained. In Section III, the proposed technique is discussed in detail. In Section IV and Section V, the experimental results are described and discussed in detail. In Section VI, a summary of the important closing remarks is provided.

II. RELATED WORK

A. SAND DUST IMAGE COLOR CORRECTION

Currently, the most used technique for image color correction is the white balance method, and examples of it include the gray world algorithm based on the RGB color space [5] and the white patch algorithm based on the YUV color space [28]. These two methods can recover image colors to some degree, but color bias remains. To address the problem, combinations of the gray world and white patch algorithms are developed in [21] and [22], where the image color is corrected based on the gray world and white patches. Retinex-based methods are developed for image color correction in [23] and [24], where the image is regarded as a product of the illumination image and the reflection image. By removing the estimated illumination image from the original image, a reflection image with a pleasing visual appearance can be obtained. In [26], a color transfer method is proposed that transfers the color of a clear image that has the highest similarity with the sand dust image, which obtains a normal color image.

B. SAND DUST IMAGE CONTRAST ENHANCEMENT

Although the optical imaging process is more intricate in a sand dust environment than a hazy environment, sand dust images are similar to hazy images in some optical characteristics, such as atmospheric scattering and absorption. Considering this point, many researchers applied dehazing methods for sand dust image enhancement, including histogram equalization [1]–[6], Retinex methods [7], the Laplacian filter [8], Nonlinear functions such as the Gamma function [9], [10], various image prior (such as the dark channel prior (DCP), color attenuation prior, and sparse prior)-based methods [11]–[17], [34], and various deep learning-based methods [18]–[20]. Of these methods, the DCP-based method [12] has received considerable attention due to its effectiveness in most haze scenarios. For example, Yu *et al.* [15] proposed a method based on the DCP and information loss constraint for single sand-dust degraded image recovery. Huang et al. presented restoration methods for hazy and sandstorm images using adaptive Gamma correction and the dark channel prior [10], [31] where adaptive Gamma correction is used to solve the transmission overestimation that is caused by the low observed intensity due to color casts.

Though there are varying degrees of success for enhancing image contrast, the DCP-based method that is mentioned above suffers from the following problems.

(1) It fails to restore heavily tinted sandstorm images because most blue light is scattered and absorbed, which causes the DCP to fail, and leads to inaccurate ambient light and transmission estimations.

(2) Over-enhancing or under-enhancing images with large sky or white object areas and underexposure in shadow regions because of not considering the inhomogeneous atmospheric light and color cast.

Aiming at problems that were mentioned above, we develop an improved dehazing method based on the dark channel prior for sand dust degraded image enhancement in the following Section.

III. THE PROPOSED METHOD

Figure 2 details our proposed method. It includes three models in sequence: color correction, dust haze removal and

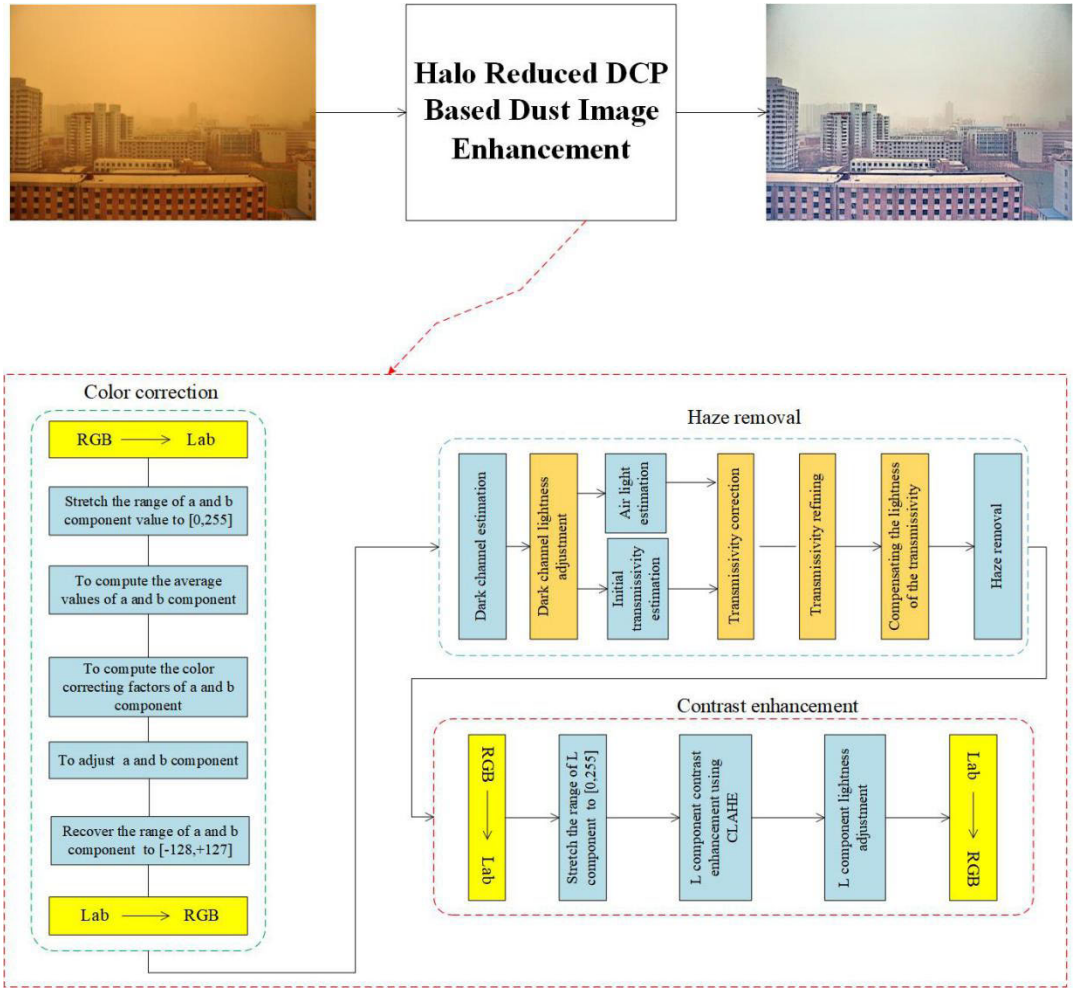

FIGURE 2. Illustration of the proposed method.

illumination adjustment. The input sand dust images are first converted into the LAB color space from the RGB color space. Then, a white balance algorithm in the LAB color space based on the gray world assumption is implemented to adjust the a and b chromatic components. Next, a halo-reduced dehazing method based on an improved DCP is developed for dust removal. After that, contrast stretching based on an improved CLAHE in the LAB color space is performed. To obtain prominence to improve on the artifacts of histogram equalization, the guided filter is followed. The details are as follows.

A. COLOR CORRECTION BASED ON GRAY WORLD ASSUMPTION

For the color correction of sand dust images, one of the most commonly used theories is the gray world theory [5]. This theory is based on the assumption that the average value of an RGB color image in each color channel is equal. Viz., the average value of a normal color image is gray. Assuming that Rav, Gav, and Bav respectively represent the average value of the R, G, and B color channels in an image, and Rc, Gc, and Bc respectively represent the corrected values of the R, G, and B color channels, we have the following:

$$\begin{cases} \mathrm{R_c} = R\dfrac{G_{av}}{R_{av}} \\ \mathrm{G_c} = G \\ \mathrm{B_c} = B\dfrac{G_{av}}{B_{av}} \end{cases} \tag{1}$$

However, because the transformation of a different image channel in the RGB color space is not a linear transformation, the color for pixels with the same color but different brightnesses will be different after their revision using equation (1), and this will cause a distorted color correction in the RGB color space.

In comparison, the color transformation in the LAB color space is a linear variation of the color of components a and b. Here, a positive value of a represents red and a negative one represents green. In addition, a positive value of b represents yellow and a negative one represents blue. Notably, the colors of the pixels are determined only by components a and b, and there is no relation to the brightness. As a result, the colors

for pixels with the same color and different brightnesses will also be the same color and without any color distortion after the adjustment of components a and b. Therefore, the LAB color space can provide a better solution for the color transformation than the RGB color space.

Given the above analyses, in this work, we address the color correction in the LAB color space. We assume that Aav and Bav respectively represent the average values of components a and b in the LAB color space, and Ac and Bc respectively represent the corrected values of components a and b. Based on the gray world theory, we form the corrected image color in the LAB color space as

$$\begin{cases} \mathrm{A_c} = \mathrm{A\text{-}A_{av}} \\ \mathrm{B_c} = B\text{-}\mathrm{B}_{av} \end{cases} \tag{2}$$

B. DUST HAZE REMOVAL USING HALO-REDUCED DEHAZING METHOD BASED ON DCP

Due to the similar optical characteristics of sand dust images to hazy images, the following widely used haze image model is used to describe the formation of a dust image and dust-free image:

$$\mathrm{I}(x) = J(x)t(x) + A(1 - t(x)) \tag{3}$$

where J(x) denotes the scene radiance at 2D location x; A is the ambient light in the atmosphere, which is referred to as the airlight and is typically approximated as the color of the sky; and t(x) is the transmission at 2D location x. Here, t(x) is commonly written as an exponential decay term of light attenuation as

$$\mathrm{t}(x) = e^{-\beta d(x)} \tag{4}$$

in which $d(x) \geq 0$ is the distance between the scene point and the camera, and β is the spectral attenuation coefficient.

In equation (3), the observed radiance I(x) can be regarded as the blending of the scene radiance J(x) and A, which is controlled by transmission t(x). The term A(1−t(x)) represents the additional light that is scattered in the line of sight as a result of the reflected solar light from floating aerosols, and the term J(x)t(x) represents the amount of scene irradiance that managed to reach the camera without being scattered.

From equation (3), it can be seen that to restore the dust haze-free image, the key is to obtain the image atmospheric transmittance t(x) and the atmospheric light intensity A.

To estimate the image atmospheric transmittance t(x), He presented a state of art method based on the DCP in [12]. It is based on the observation that in haze-free non-sky outdoor images, some RGB color channels (at least one) have very low intensities at some pixels. I.e.,

$$\mathrm{J}^{dark}(x) = \min_{c\in\{r,g,b\}} \left(\min_{y\in\Omega(x)} (\mathrm{J}^c(\mathrm{x})) \right) \approx 0 \tag{5}$$

where $\mathrm{J}^{\mathrm{dark}}(x)$ represents a dark channel of J(x), J^{c} represents a color channel of J(c), and $\Omega(x)$ is a local patch that is centered at x.

After taking the minimum operation among the three RGB color channels in the local patch on the hazy images using equation (3), we obtain the following:

$$\min_{c\in\{r,g,b\}} \left(\min_{y\in\Omega(x)} \left(\frac{\mathrm{I}^c(\mathrm{x})}{\mathrm{A}^{\mathrm{c}}}\right)\right) = \min_{c\in\{r,g,b\}} \left(\min_{y\in\Omega(x)} \left(\frac{\mathrm{J}^c(\mathrm{x})}{\mathrm{A}^{\mathrm{c}}}\right)\right) t(x) + (1 - t(x)) \tag{6}$$

From equations (5) and (6), t(x) can be obtained using the following formula:

$$t(x) = 1 - \frac{I^{dark}(x)}{A} \tag{7}$$

This formula is widely used to estimate the image atmospheric transmittance t(x) in existing dehazing methods [12], [15]. However, from equation (4), we know that the value of the transmission t(x)≥0. Nevertheless, in the case of an image with a large sky region or white objects, because $A < I^{dark}(x)$, from equation (7), we can see that t(x) will yield a negative value, which results in severe color distortion in the restored image. To address this problem, we rewrite formulation (7) as

$$t(x) = 1 - \omega \frac{I^{dark}(x)}{max(A, 1 - A)} \tag{8}$$

where ω is a constant, which is used to describe the dust concentration, and usually $0 < \omega < 1$. In this work, we set $\omega = 0.95$. With formula (8), we can avoid a negative t(x).

Note that abovementioned transmission t(x) is estimated based on a local constant hypothesis that the pixels in a local image patch have the same value. However, the pixels in a local image patch will not always share a similar depth value. Therefore, the assumption will fail in areas with abrupt depth changes. In such a case, halo effects would be introduced in the depth discontinuities. In addition, the original DCP in [12] assumes that the outdoor images do not have sky regions, but this is not always true. Furthermore, if an outdoor image has a large sky region, the estimation of t(x) using formula (8) will be incorrect, which will introduce color distortions and artifacts in sky regions. To overcome these two problems, we introduce two constraints to formula (8) and rewrite it as

$$t'(x) = \min(v. * \max(t(x), t_0), 1) \tag{9}$$

where t0 is a constant that is used to restrict the atmospheric transmission t(x) to a lower bound (in this paper, t0=0.1). Parameter v is a constraint variable, which is used to reduce the distortion, and it is defined as

$$v = \max\left(\mathrm{k} \Big/ (mean(J(x)) - A), 1\right) \tag{10}$$

where k is a constant that is used to control the transmittance tolerance in sky regions.

To refine the estimated transmission, a guided filter [33] is applied.

To estimate the value of airlight A, existing methods typically determine the airlight value based on the brightest pixels in an image [12]. This estimate is compromised when objects

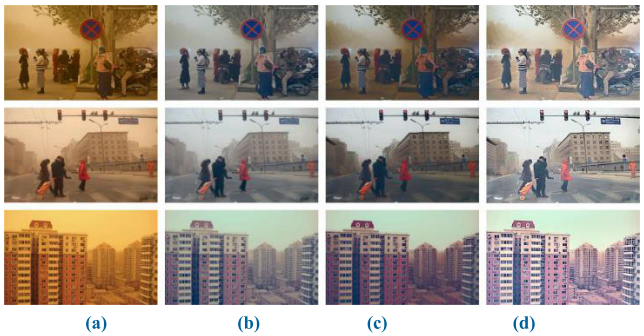

FIGURE 3. Illustration of sand dust image enhancement results using our proposed method. (a) Input sand dust image, (b) color recovered images, (c) dust haze removed images, and (d) final output images with our method.

that are brighter than the sky are present in the scene and lead to the identification of some blocks in the bright non-sky objects as airlight, thereby resulting in color shifts in the output images. Additionally, if the atmospheric light is too large, the restored images will be dim. To overcome this problem, in this paper, the following method is used. First, we obtain the pixels with the 0.1% brightest values in the dark channel and then obtain the corresponding pixels of the 0.1% dark channel pixels in the R, G, and B channels of the input dust images, respectively. Finally, we take the median of the largest pixel values of the 3 channels of I(x) as the global atmospheric light A.

Once the final transmission t'(x) and atmospheric light A are estimated, the dust-free image can be obtained using the simple inversion of equation (3) as follows:

$$J(x) = \frac{I(x) - A}{t'(x)} + A \tag{11}$$

where t0 is a constant that is used to restrict the atmospheric transmission t(x) to a lower bound.

C. ILLUMINATION ADJUSTMENT

Because underexposure still exists in an image after color correction and dust removal, as shown in Figure 3 (b), illumination adjustment is applied as a postprocessing operation in this section. For this purpose, we first convert the color corrected and dust removal images from the RGB color space to the LAB color space. Then, we exploit the L channel of the LAB color space to adjust the illumination using a Gamma function improved contrast limited adaptive histogram equalization (CLAHE). CLAHE is a modification of the traditional adaptive histogram equalization that applies the contrast limiting procedure for each neighborhood to derive a transformation function. However, this may also cause unbalanced contrast in the enhanced image due to increasing the brightness of the degraded image too much. To overcome this problem, we introduce the Gamma function to improve the CLAHE. The purpose of using the Gamma function in our work is similar to that in Ancuti's work [35].

The Gamma function [27] is a gray-level transformation function that describes the relationship between a pixel's luminance and its numeric value, and it is applied to images to enhance their imperfect luminance. R is the Gamma-corrected image, X is the original image in which the pixel values range from 0 to 1, c is a positive constant parameter that is used to control the brightness, and γ is a positive constant parameter that represents the Gamma value. Then, the Gamma function can be defined as

$$\mathrm{R} = \mathrm{cX}^{\gamma} \tag{12}$$

The advantage of the power-law transformation is that the transformation function can be controlled by varying the Gamma γ values. Its disadvantage is that increasing γ would overcompensate the image's Gamma and thereby darken the processed image while enhancing its contrast. Therefore, we must expand this dynamic range to fit its full natural interval. For this purpose, in this study, to minimize the disadvantage of the traditional Gamma function, we propose a normalized Gamma correction (NGC). Using normalization, the new Gamma function can account for the full dynamic range of normalization to reduce the brightness contrast enhancement. The NGC equation is written as follows:

$$\mathrm{NGC} = \frac{[\mathrm{R\text{-}min}(R)]}{[\max(R) - \min(R)]} \tag{13}$$

As a final point, we add the NGC function to CLAHE. As a consequence, the increased brightness and the unbalanced contrast of CLAHE are adjusted and an adequate visual quality for the processed images is attained.

IV. EXPERIMENTS

In this section, we present the experimental details, including the data set, the parameter setting, the quality measures, and the evaluation results.

A. DATA SET AND PARAMETER SETTING

To evaluate whether our proposed method can obtain the closest image to its corresponding original one, we construct a sand dust image set in this section. Our original images come from O-HAZE [40], which is a public haze image set that consists of pairs of haze/haze-free images. Although sand dust images are similar to hazy images with respect to some optical characteristics, such as atmospheric scattering and absorption, the optical imaging process is more intricate in the sand dust environment than that in the haze environment. The most obvious difference between them is that sand dust images usually have an overall yellow tone. Therefore, for simplicity, we model the sand dust condition only by changing the color tone of hazed images in O-HAZE. Adobe Photoshop is used and we try different kinds of parameters to make the hazed image color tone fit the result in sand dust conditions. Finally, we resize these images to 400×600 and convert them to the Portable Network Graphics format.

To evaluate the proposed method on real sand dust images, we created a data set that consists of 250 sand dust images that were collected from the Internet.

The proposed method in this paper is compared with several recent state-of-the-art methods that used for sand dust image enhancement, including CLAHE [29], Wang's work [8], and MSRCR (Multi-Scale Retinex with Color Restoration) [30].

Because our method is inspired by He's DCP [12] and because sand dust images are similar to hazy images with respect to some optical characteristics, to test whether other dehazing methods can obtain similar results to those from our method, we also compare our method with several popular dehazing methods, including He's method [12], Meng's method, Fattal's method, Tarl's method, and Fu's method.

The software implementations of these methods were provided by the authors and input into MATLAB. We use the default parameters that are reported in these three papers.

All experiments are performed on a PC with an Intel Core i9-9900K @ 3.60 GHz Core i5 CPU, 32GB of RAM and an Nvidia GeForce RTX 2080 Ti.

B. VALIDATION OF THE IMAGE ENHANCEMENT EFFECT OF THE PROPOSED METHOD

Figure 3 illustrates part of the results that are obtained with our proposed method, where Figure 3(a) is input sand dust images, Figure 3(b) is the color correction results using our method, Figure 3(c) is the dust removed results using our improved DCP dehazing method, and Figure 3(d) is the final results using our method. As seen after applying our image color correction method on the input sand dust images, the color deviations of the input sand dust images are well recovered. However, haze remains where rich image details cannot be observed, as shown in Figure 3(b). After the dust removal using our improved DCP dehazing method, though most dust has been removed, the images are still underexposed, and their contrast is very poor, as shown in Figure 3(c). In comparison, in the final results using our method, the image contrast and brightness are both significantly enhanced and images with rich details and vivid normal colors are obtained, as shown in Figure 3(d).

C. QUALITATIVE EVALUATION USING REAL SAND DUST IMAGES

Figure 4 illustrates the comparisons of our method with CLAHE [29]. The middle column is the CLAHE results, and the right column is results using our method. It can be observed that our method can remove the overall yellow color from sand dust images and obtain a color natural image with enhanced contrast. In comparison, the overall yellow color remained in the CLAHE results, and obvious halos appeared around the trees or people, which resulted in poor visuals. In the sky region, there are also obvious artifacts and color distortions.

In addition, we also compare our proposed method with CLAHE in a fair way. That is, before applying CLAHE to dust image enhancement, all input sand dust images are color corrected using the same color correction method that is used in our method. Figure 5 shows this comparison results. It can be observed that all results in this experiment show that the overall yellow color from the input sand dust images has been removed, and we obtain natural color images with enhanced contrast. However, the results using CLAHE are blurrier and dimmer than those from our proposed method. In addition, in the sky regions or regions around the people in the images that are obtained using CLAHE, there are also obvious artifacts. This result confirms our observations from Figure 4.

Figure 6 compares our method with Wang's work [8]. It can be observed that both Wang's method and our method can well recover the colors of the input sand dust images. However, in the recovered images using Wang's method, obvious halo artifacts appear, such as in the areas surrounding the heads of people and lamps and the areas around the leaves of trees, as shown in the middle column. In comparison, there are no halo artifacts in our results, and the images' brightness and details are also significantly augmented, as shown in the left column.

FIGURE 4. Comparisons of our method with CLAHE [29]. left column: Sand dust images, middle column: CLAHE [29], and right column: Results using our method.

FIGURE 5. Comparisons of our method with CLAHE [29] in a fair way. left column: Sand dust images, middle column: CLAHE [29], and right column: Results using our method.

FIGURE 6. Comparisons of our method with Wang's work [8]. left column: Sand dust images, middle column: Wang's work [29], and right column: Results using our method.

FIGURE 7. Comparisons of our method with the MSRCR [30]. left column: Sand dust images, middle column: MSRCR [30], and right column: Results using our method.

Figure 7 compares our approach with the MSRCR (Multi-Scale Retinex with Color Restoration) [30], where the left column is input sand dust images, the middle column is the MSRCR results, and the right column is the results using our method. As seen in the middle column in Figure 6, the contrast is significantly enhanced, but the color deviation, distortion, and halo artifacts are also serious. In comparison, our results are very visually pleasing.

D. QUALITATIVE EVALUATION USING SYNTHESIZED SAND DUST IMAGES

To verify the method's effectiveness for complete images, the proposed method is also evaluated using synthesized sand dust images by comparing it with other state-of-the-art sand dust image enhancement methods that were mentioned above. The sand dust images are synthesized by changing the color tone of the hazed images using O-HAZE in Adobe Photoshop.

Figure 8 compares our method with CLAHE [29]. Here, Figure 8 (a) is the synthesized sand dust images, Figure 8(b) is the results using CLAHE, Figure 8(c) is the results using color correction+CLAHE, Figure 8(d) is the results using our method, and Figure 8(e) is the ground truths. It can be observed that our method can remove the overall yellow color from sand dust images and obtain a natural-color image with enhanced contrast, which is more consistent with the ground truths. In comparison, the overall yellow color remained in the results using CLAHE. Though the color correction+CLAHE method has removed the overall yellow color from the synthesized sand dust images, the results are still too blurry to observe. In addition, there are also obvious artifacts and color distortions, and the results are visually far from the ground truths.

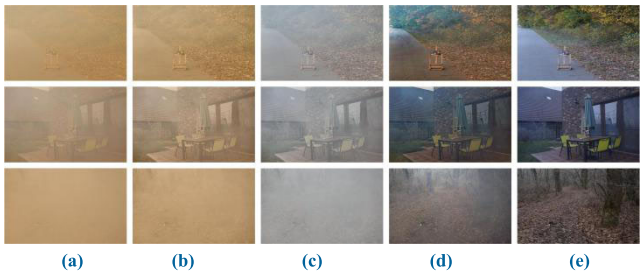

FIGURE 8. Comparisons of our proposed method using CLAHE [29] on synthesized sand dust images. (a) Input synthesized sand dust images, (b) results using CLAHE, (c) results using color correction+CLAHE, (d) results using our method, and(e) ground truths.

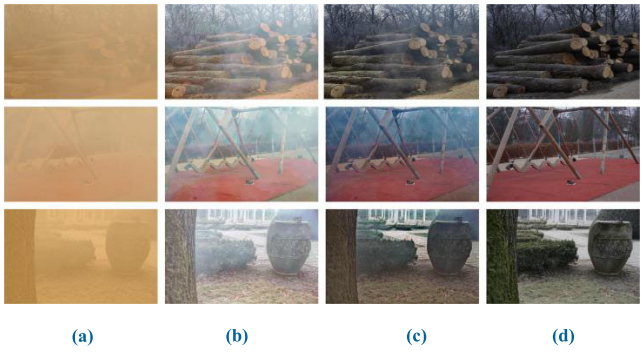

FIGURE 9. Comparisons of our method with Wang's work [8]. (a) Synthesized sand dust images, (b) results using Wang's work [8], (c) results using our method, and (d) the ground truths.

Figure 9 compares our method with Wang's work [8], where Figure 9 (a) is the synthesized sand dust images, Figure 9(b) is the results using Wang's work [8], Figure 9(c) is the results using our method, and Figure 9(d) is the ground truths. It can be observed that both Wang's method and our method can well recover the colors of synthesized sand dust images. However, in the images that were recovered using Wang's method, obvious haze remains, and the images look to be slightly blurry. In comparison, the images' brightness and details are significantly augmented using our method, which is more similar to the ground truths than those using Wang's method.

Figure 10 compares our approach with the MSRCR [30], where Figure 10 (a) is the synthesized sand dust images, Figure 10(b) is the results using the MSRCR, Figure 10(c)

FIGURE 10. Comparisons of our method with the MSRCR [30]. (a) Synthesized sand dust images, (b) results using the MSRCR, (c) results using our method, and (d) ground truths.

TABLE 1. Comparison of our method with different state-of-the-art sand dust image enhancement methods using synthesized sand dust images.

	SSIM	MSE
CLAHE	0.9873	0.1017
Wang's method [8]	0.9898	0.0723
MSRCR [30]	0.9924	0.0596
Our method	0.9972	0.0211

is results using our method, and Figure 10(d) is the ground truths. As seen from Figure 10(b), the contrast is significantly enhanced, but the color deviations, distortions, and halo artifacts are serious. In comparison, our results are much more visually pleasing and closer to the ground truths than those using the MSRCR.

E. QUANTITATIVE EVALUATION

To quantitatively evaluate the performance of our proposed method on the synthetic data, the SSIM (Structural Similarity) and the MSE (mean squared error) [33] measures are employed in this experiment. The structural similarity (SSIM) image quality assessment index evaluates the ability of an algorithm to preserve the structural information. The mean squared error (MSE) indicates the average difference between the recovered image and the reference ground truth image. In general, a higher SSIM means better structural similarity between the recovered image and the ground truth image, and a lower MSE represents that the recovered image is more acceptable.

Table 1 shows the comparisons of our method with the above mentioned state-of-the-art sand dust image enhancement methods on the synthesized sand dust images in terms of the average SSIM and average MSE. It can be seen that our method obtained the largest SSIM and the smallest MSE. This result is consistent with the qualitative evaluation using the synthesized sand dust images.

TABLE 2. Comparison of our method with different state-of-the-art sand dust image enhancement methods using real sand dust images.

		e	σ	$\bar{r}$
Top row	CLAHE	0.5335	0.0071	0.44556
	Wang's	0.4268	0.0071	0.5451
	MSRCR	0.4105	0.0071	0.5227
	Our	05792	0.0071	0.5843
Middle row	CLAHE	0.9071	0	0.3410
	Wang's	0.9008	0	0.2673
	MSRCR	0.9134	0	0.2123
	Our	0.9229	0	0.4627
Bottom row	CLAHE	0.4281	0.4878	0.6112
	Wang's	0.2834	0.4878	0.6610
	MSRCR	0.1722	0.4878	0.7072
	Our	0.5319	0.4878	0.8202

To quantitatively evaluate the performance of the different methods on real-world images, since the ground truth images are not available, the following three measures are used in this paper: the percentage of new visible edges e, the contrast restoration quality $\bar{r}$, and the saturation σ [39]. The percentage of new visible edges e represents the edges that are newly visible after restoration, the contrast restoration quality $\bar{r}$ measures the mean ratio of the gradients at the visible edges, and the saturation σ computes the percentage of pixels that become completely black or completely white after restoration. A higher e and a σ closer to zero imply better performance, and a higher $\bar{r}$ implies stronger recovery of the local contrast.

Table 2 shows the comparisons of our method with the above mentioned state-of-the-art sand dust image enhancement methods on real sand dust images using the percentage of new visible edges e, the contrast restoration quality $\bar{r}$, and the saturation σ. The corresponding images are shown in Figure 11. It can be seen that except for σ, which is the same for all methods and nearly close to zero, our method has obtained the highest e and $\bar{r}$ on all images in Figure 11. This implies the superior performance for our method, which is consistent with the qualitative evaluation of the images in Figure 11.

Overall, the qualitative and quantitative comparison results in Figure 4-Figure 11 and Table 1-Table 2 demonstrate that our method has advantages over the other state-of-the-art sand dust image enhancement methods in terms of removing dust haze, improving visibility, and compensating for the illumination while avoiding most of the negative effects.

FIGURE 11. Comparisons of our method with several state-of-the-art sand dust image enhancement methods. (a) Synthesized sand dust images, (b) results using CLAHE, (c) results using Wang's method, (d) results using the MSRCR, and (e) results using our method.

V. DISCUSSIONS

Our method is based on an improved DCP dehazing method. To verify whether our improved DCP can be replaced with other dehazing methods, we compare our improved DCP with several popular dehazing methods, including He's original DCP method [12], Tarel's method [37], Meng's method [38], and Cai's method [19]. Of these, Tarel and Hautiere [37] uses the median filter to mat the dark channel map. Meng *et al.* [38] applies the inherent boundary constraint to restore the image. Cai's method [19] uses a CNN to generate nearly all haze-relevant features. For fairness, all dehazing methods are compared under the same conditions. That is, before dust haze removal, all sand dust images are color corrected using the same color correction method, and after dust haze removal, their illuminations are also adjusted using the same CLAHE method in the same way.

Figure 12 shows the comparison results of different dehazing methods using synthesized sand dust images, of which Figure 12 (a) is the synthesized sand dust images, Figure 12(b) is the results using He's DCP [12], Figure 12(c) is the results using Tarel's method [37], Figure 12(d) is the results using Meng's method [38], Figure 12(e) is the results using Cai's CNN method [19], Figure 12(f) is the results using our method, and Figure 12(g) is the ground truths.

From Figure 12, it can be observed that there is still obvious haze in the recovered images using both Tarel's method [37] (as shown in Figure 12(c)) and Cai's CNN method [19] (as shown in Figure 12(e)) where the images are slightly dim and blurry. In contrast, He's [12] method can significantly improve the visual effect of the hazy images, but the color shift phenomenon still exists in the regions with white objects because the dark channel has bright values near such objects. The results using Meng's method look unnatural. Compared with the results of the above mentioned methods, our method has better performance in terms of its haze removal ability and visual effect (see Figure 12(f)), and its results are the closest to the ground truths.

Table 3 shows the quantitative comparisons of the above mentioned methods using Figure 12. It can be seen that our method obtained the largest SSIM, e and $\bar{r}$ and the smallest MSE and σ on all images in Figure 12. This implies the superior performance for our method, which is consistent with the qualitative evaluation from Figure 12.

TABLE 3. Quantitative comparison of our method with popular dehazing methods using synthesized sand dust images.

		e	σ	$\bar{r}$	SSIM	MSE
Top row	He	0.9955	0.00	0.5805	0.9953	0.0334
	Tarel	0.9905	0.00	0.3896	0.9842	0.1140
	Meng	0.9963	0.00	0.5813	0.9959	0.0298
	Cai	0.9544	0.00	0.2903	0.9906	0.0678
	Our	**0.9979**	**0.00**	**0.5815**	**0.9980**	**0.0148**
Middle row	He	0.9905	0.00	0.5140	0.9971	0.0214
	Tarel	0.9740	0.00	0.1619	0.9800	0.1479
	Meng	0.9926	0.00	0.4683	0.9978	0.0159
	Cai	0.9723	0.00	0.1206	0.9920	0.0593
	Our	**0.9940**	**0.00**	**0.5149**	**0.9991**	**0.0077**
Bottom row	He	0.9895	0.00	0.5795	0.9958	0.0313
	Tarel	0.9823	0.00	0.4659	0.9756	0.1765
	Meng	0.9901	0.00	0.5793	0.9965	0.0268
	Cai	0.9781	0.00	**0.5763**	0.9911	0.0657
	Our	**0.9920**	**0.00**	**0.5785**	**0.9974**	**0.0206**

According to the basic structure, the image color space can be classified as the primary color space and the color-brightness separation color space. For the former, the typical one is the RGB color space, and the latter includes the YUV color space and LAB color space. To verify whether the LAB color space that is adopted in this paper is the best color space for sand dust color correction, we compared the LAB color space with other color spaces in this section. The experimental results are shown in Figure 13, of which Figure 13 (a) is the input sand dust images, Figure 13(b) is the results using the RGB color space, Figure 13(c) is results using the YUV color space, and Figure 13(d) is the results using the LAB color space. It can be seen that there are obvious artifacts in the images of Figure 13(b) and color distortion in the images of Figure 13(c). In comparison, the colors of the images in Figure 13(d) look more natural. These results show that the LAB color space is better than the other two color spaces in sand dust image color recovery.

To verify whether our proposed NGC improved CLAHE is truly better than the original CLAHE at adjusting the illumination, we compare the NGC improved CLAHE with the original CLAHE in Figure 14. In Figure 14, the left column is the original input sand dust images, the middle column is the illumination adjustment results using the original CLAHE, and the right column is the results using our NGC improved CLAHE. For fairness, except for the use of

FIGURE 12. Comparisons of our method with popular dehazing methods using synthesized sand dust images. (a) Synthesized sand dust images, (b) results using He's DCP [12], (c) results using Tarel's method [37], (d) results using Meng's method [38], (e) results using Cai's CNN method [19], (f) results using our method, and (g) ground truths.

FIGURE 13. Comparisons of sand dust image color correction using different color spaces. (a) Input sand dust images, (b) results using the RGB color space, (c) results using the YUV color space, and (d) results using the LAB color space.

FIGURE 14. Comparisons of our proposed NGC improved CLAHE with the original CLAHE. left column: Sand dust images, middle column: Illumination adjustment results using the original CLAHE, right column: Illumination adjustment results using our NGC improved CLAHE.

the NGC CLAHE or the use of the original CLAHE, the other sand dust image enhancement methods are all the same. It can be observed that the contrast of the images in the middle column is unbalanced, and part of the details, such as the faces in the image on the top row and the feet in the image on the bottom row, are too dark to observe. With respect to the images in the right column, both the contrast and brightness of all images are balanced, and the details are obviously observed. These results demonstrate that our method is better than the original CLAHE at adjusting the illumination.

VI. CONCLUSIONS

In this paper, a method based on halo-reduced DCP dehazing for sand dust image enhancement is proposed. It includes three components in sequence: gray world color correction in the LAB color space, dust removal using an improved halo reduced DCP dehazing method, and contrast stretching in the LAB color space based on the improved CLAHE, in which the guided filter is applied to improve the artifacts from histogram equalization. Experiments on a large number of real sand dust images demonstrate that the proposed method can acquire good color fidelity and proper brightness.

Although our approach works well for most outdoor sand dust images, it may fail in some extreme cases. Future work will focus on some exceptional cases where a dust patch has similar features with a dust-free one, causing all existing enhancement approaches to fail. To address such cases, we will focus on using deep learning methods in our next work.

REFERENCES

[1] T. Yan, L. J. Wang, and J. X. Wang, "Method to enhance degraded image in dust environment," *J. Softw.*, vol. 9, no. 10, pp. 2672–2677, Oct. 2014.

[2] J.-Y. Kim, L.-S. Kim, and S.-H. HWang, " An advanced contrast enhancement using partially overlapped sub-block histogram equalization," *IEEE Trans. Circuits Syst. Video Technol.*, vol. 11, no. 4, pp. 475–484, Apr. 2001.

[3] Q. Liu, M. Chen, and D. Zhou, "Single image haze removal via depth-based contrast stretching transform," *Sci. China Inf. Sci.*, vol. 58, no. 1, pp. 1–17, Jan. 2015.

[4] T. Yan, L.-J. Wang, and J. X. Wang, "Video image enhancement method research in the dust environment," *Laser J.*, vol. 35, no. 4, pp. 23–25, Jun. 2014.

[5] J. Wang, Y. Pang, Y. He, and C. Liu, "Enhancement for dust-sand storm images," in *Proc. 22nd Int. Conf. Multimedia Model.*, New York, NY, USA, 2016, pp. 842–849.

[6] N. Zhi, S. J. Mao, and M. Li, "Visibility restoration algorithm of dust-degraded images," *J. Image Graph.*, vol. 21, no. 12, pp. 1585–1592, Nov. 2016.
[7] H. Gao, P. Wei, and J. Ke, "Color enhancement and image defogging in HSI based on Retinex model," in *Proc. Int. Conf. Opt. Instrum. Technol., Optoelectron. Imag. Process. Technol.*, Beijing, China, 2015, Art. no. 962203.
[8] J. Wang, Y. Pang, Y. He, and C. Liu, "Enhancement for dust-sand storm images," in *Proc. Int. Conf. Multimedia Model.*, Miami, FL, USA, 2016, pp. 842–849.
[9] S.-C. Huang, F.-C. Cheng, and Y.-S. Chiu, "Efficient contrast enhancement using adaptive gamma correction with weighting distribution," *IEEE Trans. Image Process.*, vol. 22, no. 3, pp. 1032–1041, Mar. 2013.
[10] S.-C. Huang, B.-H. Chen, and W.-J. Wang, "Visibility restoration of single hazy images captured in real-world weather conditions," *IEEE Trans. Circuits Syst. Video Technol.*, vol. 24, no. 10, pp. 1814–1824, Oct. 2014.
[11] R. T. Tan, "Visibility in bad weather from a single image," in *Proc. IEEE Conf. Comput. Vis. Pattern Recognit. (CVPR)*, Anchorage, AK, USA, Jun. 2008, pp. 1–8.
[12] K. He, J. Sun, and X. Tang, "Single image haze removal using dark channel prior," *IEEE Trans. Pattern Anal. Mach. Intell.*, vol. 33, no. 12, pp. 2341–2353, Dec. 2011.
[13] Q. Zhu, J. Mai, and L. Shao, "A fast single image haze removal algorithm using color attenuation prior," *IEEE Trans. Image Process.*, vol. 24, no. 11, pp. 3522–3533, Nov. 2015.
[14] S. G. Narasimhan and S. K. Nayar, "Contrast restoration of weather degraded images," *IEEE Trans. Pattern Anal. Mach. Learn.*, vol. 25, no. 6, pp. 713–724, Jun. 2003.
[15] S. Yu, H. Zhu, J. Wang, Z. Fu, S. Xue, and H. Shi, "Single sand-dust image restoration using information loss constraint," *J. Modern Opt.*, vol. 63, no. 21, pp. 2121–2130, May 2016.
[16] Z. H. Shi, M. Zhu, X. Zheng, and M. Zhao, "Fast single-image dehazing method based on luminance dark prior," *Int. J. Pattern Recognit. Artif. Intell.*, vol. 31, no. 2, pp. 1–9, Dec. 2017.
[17] X. Fu, Y. Huang, D. Zeng, X.-P. Zhang, and X. Ding, "A fusion-based enhancing approach for single sandstorm image," in *Proc. IEEE 16th Int. Workshop Multimedia Signal Process.*, Jakarta, Indonesia, Sep. 2014, pp. 1–5.
[18] K. T. Tang, J. C. Yang, and J. Wang, "Investigating haze-relevant features in a learning framework for image dehazing," in *Proc. IEEE Int. Conf. Comput. Vis. Pattern Recognit.*, Columbus, OH, USA, Jun. 2014, pp. 2995–3000.
[19] B. Cai, X. Xu, K. Jia, C. Qing, and D. Tao, "DehazeNet: An end-to-end system for single image haze removal," *IEEE Trans. Image Process.*, vol. 25, no. 11, pp. 5187–5198, Nov. 2016.
[20] W. Ren, S. Liu, H. Zhang, J. Pan, X. Cao, and M.-H. Yang, "Single image dehazing via multi-scale convolutional neural networks," in *Proc. Eur. Conf. Comput. Vis.*, Amsterdam, The Netherlands, 2016, pp. 154–169.
[21] A. Rizzi, C. Gatta, and D. Marini, "Color correction between gray world and white patch," *Proc. SPIE*, vol. 4662, pp. 367–375, May 2002.
[22] P. Getreuer, "Automatic color enhancement (ACE) and its fast implementation," *Imag. Process. Line*, vol. 2, pp. 266–277, Nov. 2012.
[23] K. J. Kwon and Y. H. Kim, "Scene-adaptive RGB-to-RGBW conversion using retinex theory-based color preservation," *J. Display Technol.*, vol. 8, no. 12, pp. 684–689, Dec. 2012.
[24] L. Kratz and K. Nishino, "Factorizing scene albedo and depth from a single foggy image," in *Proc. IEEE 12th Int. Conf. Comput. Vis.*, Kyoto, Japan, Sep./Oct. 2009, pp. 1701–1708.
[25] A. Jun and M. Chunbo, "Adaptive stretching method for underwater image color correction," *Int. J. Pattern Recognit. Artif. Intell.*, vol. 32, no. 2, 2018, Art. no. 1854001.
[26] H. Liu, C. Li, Y. Wan, and Y. Zhang, "Dust image enhancement algorithm based on color transfer," in *Proc. Chin. Conf. Comput. Vis.*, Tianjin, China, 2017, pp. 168–179.
[27] C.-M. Tsai, "Adaptive local power-law transformation for color image enhancement," *Appl. Math. Inf. Sci.*, vol. 7, no. 5, pp. 2019–2026, Sep. 2011.
[28] R. Z. Zhou, J. He, and Z. L. Hong, "Adaptive algorithm of auto white balance for digital camera," *J. Comput. Aided Des. Comput. Graph.*, vol. 17, no. 3, pp. 529–533, Mar. 2005.
[29] K. Zuiderveld and P. Heckbert, "Contrast limited adaptive histogram equalization," in *Graphics Gems IV*. New York, NY, USA: Academic, 1994.
[30] D. J. Jobson, Z.-U. Rahman, and G. A. Woodell, "A multiscale Retinex for bridging the gap between color images and the human observation of scenes," *IEEE Trans. Image Process.*, vol. 6, no. 7, pp. 965–976, Jul. 1997.
[31] S.-C. Huang, J.-H. Ye, and B.-H. Chen, "An advanced single-image visibility restoration algorithm for real-world hazy scenes," *IEEE Trans. Ind. Electron.*, vol. 62, no. 5, pp. 2962–2972, May 2015.
[32] Y.-T. Peng and P. C. Cosman, "Single image restoration using scene ambient light differential," in *Proc. IEEE Int. Conf. Image Process. (ICIP)*, Sep. 2016, pp. 1953–1957.
[33] Z. Shi, Y. Li, C. Zhang, M. Zhao, Y. Feng, and B. Jiang, "Weighted median guided filtering method for single image rain removal," *EURASIP J. Image Video Process.*, vol. 2018, May 2018, Art. no. 35. doi: 10.1186/s13640-018-0275-9.
[34] Y. Chang, L. Yan, and S. Zhong, "Transformed low-rank model for line pattern noise removal," in *Proc. ICCV*, Oct. 2017, pp. 1726–1734.
[35] C. O. Ancuti, C. Ancuti, C. De Vleeschouwer, and P. Bekaert, "Color balance and fusion for underwater image enhancement," *IEEE Trans. Image Process.*, vol. 27, no. 1, pp. 379–393, Jan. 2018.
[36] C. Ancuti, C. O. Ancuti, and C. De Vleeschouwer, "D-HAZY: A dataset to evaluate quantitatively dehazing algorithms," in *Proc. IEEE Int. Conf. Image Process.*, Phoenix, AZ, USA, Sep. 2016, pp. 2226–2230.
[37] J.-P. Tarel and N. Hautiere, "Fast visibility restoration from a single color or gray level image," in *Proc. IEEE 12th Int. Conf. Comput. Vis.*, 2009, pp. 2201–2208.
[38] G. Meng, Y. Wang, J. Duan, S. Xiang, and C. Pan, "Efficient image dehazing with boundary constraint and contextual regularization," in *Proc. IEEE Int. Conf. Comput. Vis.*, Sydney, NSW, Australia, Dec. 2013, pp. 617–624.
[39] N. Hautière, J.-P. Tarel, D. Aubert, and É. Dumont, "Blind contrast enhancement assessment by gradient ratioing at visible edges," *Image Anal. Stereology*, vol. 27, no. 2, pp. 87–95, 2008.
[40] C. O. Ancuti, C. Ancuti, R. Timofte, and C. De Vleeschouwer, "O-HAZE: A dehazing benchmark with real hazy and haze-free outdoor images," in *Proc. IEEE Conf. Comput. Vis. Pattern Recognit.*, Salt Lake City, UT, USA, Jun. 2018, pp. 754–762.

ZHENGHAO SHI received the B.S. degree in material science and engineering from Dalian Jiaotong University, Dalian, China, in 1995, the M.S. degree in computer application technology from the Xi'an University of Technology, Xi'an, China, in 2000, and the Ph.D. degree in computer architecture from the Xi'an Institute of Microelectronics, Xi'an, in 2005. In 2000, he joined the Xi'an University of Technology, where he was an Assistant Professor with the Department of Computer Science and Engineering, from 2000 to 2005. From 2006 to 2007 and from 2008 to 2009, he was on leave with the Department of Computer Science and Engineering, Nagoya Institute of Technology, Nagoya, Japan, for image research as a Postdoctoral Researcher. From 2007 to 2008, he was a Research Associate with Kurt Rossmann Laboratories for Radiologic Image Research, Department of Radiology, Division of Biological Sciences, University of Chicago. From 2016 to 2017, he was a Visiting Associate Professor with the Image Display, Enhancement, and Analysis (IDEA) Lab, Department of Radiology, Division of Biological Sciences, The University of North Carolina at Chapel Hill. Since 2006, he has been an Associate Professor with the Department of Computer Science and Engineering, Xi'an University of Technology. His research interests include neural networks for image processing and pattern recognition, computer-aided diagnosis, and image processing suggested by the human visual systems. He is a member of the ACM.

YANING FENG received the bachelor's degree in material science and engineering from the Northwest University of Technology, Xianyang, China, in 1995, the M.S. degree in computer science and engineering from the Xi'an University of Technology, Xi'an, China, in 2014, and the Ph.D. degree in material and information engineering from the Nagoya institute of Technology, Nagoya, Japan, in 2008. She is currently an Assistant Professor with the Xi'an University of Technology. Her research interest includes material image processing.

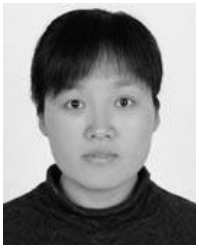

MINGHUA ZHAO received the Ph.D. degree in computer science from Sichuan University, Chengdu, China, in 2006. After that, she joined the Xi'an University of Technology, Xi'an, China, where she is currently an Associate Professor with the Department of Computer Science and Engineering. Her research interests include image processing and pattern recognition.

ERHU ZHANG received the B.S. degree in automatic control engineering from the Xi'an University of Technology, Xi'an, China, in 1987, the M.S. degree in automatic control engineering from the Xi'an University of Science and Engineering, Xi'an, in 1990, and the Ph.D. degree in biomedical engineering from Xi'an Jiaotong University, Xi'an, in 2003. He is currently a Professor with the Department of Digital media Technology, Xi'an University of Technology. His current research interests include image processing and pattern recognition.

LIFENG HE received the B.S. degree in automatic control engineering from the Northwest University of Technology, Xianyang, China, in 1982, and the M.S. and Ph.D. degrees in computer science and engineering from the Nagoya institute of Technology, Nagoya, Japan, in 1994 and 1997, respectively. He is currently a Professor with the Graduate School of Information Science and Technology, Aichi Prefectural University, Aichi, Japan. His current research fields include image processing and pattern recognition.